



Cite this: *React. Chem. Eng.*, 2021, **6**,
1462

Continuous-flow diazotization of red base KD hydrochloride suspensions in a microreaction system†

Fa-Jun Wang, An Chen, Si-da Ling and Jian-Hong Xu  *

In this work, a continuous-flow microreaction system has been developed to perform the diazotization reaction of red base KD hydrochloride in the form of a suspension solution. By investigating the effects of reaction temperature, reactant volume flow, red base KD concentration and reaction time on the diazotization reaction, the optimal reaction conditions were obtained. According to the solid–liquid reaction model, we found that the agglomeration of suspensions significantly affects the diazotization reaction due to the solid–liquid mass transfer process. Consequently, different red base KD hydrochloride suspensions were prepared under different conditions to explore the agglomeration phenomenon of the suspensions, and we observed that the crystal agglomeration could be prevented by optimizing the process of preparing the reaction suspensions. The results showed that the yield of the diazotization reaction using these optimized suspensions, which were prepared by introducing concentrated hydrochloric acid in three sequential additions of equal volume, could reach over 99% in 21.2 s at two different suspension concentrations (suspension concentration: 0.12 mol L^{-1} and 0.15 mol L^{-1}).

Received 24th February 2021,
Accepted 25th May 2021

DOI: 10.1039/d1re00075f

rsc.li/reaction-engineering

1. Introduction

Diazotization reactions are traditionally used to synthesize aryl diazonium salts, which have a wide range of applications in industries and academics.¹ Diazonium functional groups can be reduced to hydrazine or substituted by different functional groups including hydroxyl, halogen, hydrogen, etc.^{2,3} Moreover, the electrophilic diazonium functions can be attacked by nucleophiles to synthesize azo compounds.^{4,5}

The diazotization reactions are widely employed in different fields such as medicine, pesticides and other chemical industries because of their great potential in organic synthesis. For example, azo dyes and azo pigments are usually synthesized through the diazotization reaction and azo-coupling reaction.^{6–8} Aromatic fluorides are produced by the Balz–Schiemann reaction, which is a classical method for building the C–F bond *via* diazotization and fluorodediazoniation steps.⁹ Furthermore, one of the essential synthetic routes of *p*-cresol, which is a key intermediate for the synthesis of pharmaceutically active agents, is *via* the diazotization of *p*-toluidine followed by a hydrolysis reaction.¹⁰ Unfortunately, there are still many problems to be solved for the application of the diazotization reaction in

organic synthesis at the industrial scale. In general, diazotization reactions are exothermic,¹¹ ($\Delta H \sim -65$ to -150 kJ mol^{-1}), and most of the diazonium salts are unstable and easily decompose at temperature above 5 °C. Notably, in the batch process, the heat of decomposition of diazonium salts ranging from -160 kJ mol^{-1} to -180 kJ mol^{-1} may cause runaway reactions, which lead to the risk of explosion.¹²

Over the last two decades, microreaction technology has been rapidly developed and attracted a lot of attentions. It has been utilized in various industrial reactions to improve the conversion and process safety because of its inherent advantages of large specific interfacial area and short molecular diffusion distance.^{13–20} Among them, the applications of microreaction technology in the diazotization reaction are widely discussed.^{5–8,21,22}

Red base KD is an important amino-containing intermediate for the synthesis of organic pigments, such as pigment red 31, 32, 146, 147, etc.²² The diazotization reaction of red base KD is a key step for the synthesis of these pigments, and the quality of the diazonium salt has a significant impact on the quality of the final product. In addition, there are few reports in the literature on the utilization of suspensions as a reactant for the diazotization reaction in the microreaction system. Therefore, it is necessary to study the continuous-flow diazotization reaction of the red base KD hydrochloride suspensions.

In this work, a continuous-flow microreaction system has been built to perform the diazotization reaction of the

The State Key Laboratory of Chemical Engineering, Department of Chemical Engineering, Tsinghua University, Beijing 100084, China.

E-mail: xujianhong@tsinghua.edu.cn

† Electronic supplementary information (ESI) available. See DOI: 10.1039/d1re00075f

suspensions. Here, a high-pressure piston kettle was used to convey the suspensions to the microreaction system, and a membrane dispersion microreactor was used to enhance the reactant mixing. Firstly, the effects of reaction temperature, reactant volume flow, suspension concentration and reaction time on the diazotization reaction were investigated. Then, we explored the influence of the agglomeration of the suspensions on the diazotization reaction and various factors affecting the agglomeration of the suspensions. A solid–liquid reaction model was also used to describe the diazotization reaction between the red base KD hydrochloride crystal and sodium nitrite solution. Finally, the yields of the diazotization reaction using different hydrochloride suspensions prepared by different methods as reactants were compared and some operating conditions between the continuous-flow process and the traditional batch process were also compared.

2. Experimental

2.1. Materials

Red base KD (3-amino-4-methoxybenzalide) was of analytical reagent grade with a mass fraction purity of $\geq 98\%$, and it was supplied by Beijing Baierdi Biotechnology Co., Ltd. Sodium 6-hydroxynaphthalene-2-sulfonate was of technical grade with a mass fraction purity of $\geq 97\%$. It was supplied by Shanghai Macklin Biochemical Technology Co., Ltd. Hydrochloric acid was of analytical reagent grade with a mass fraction purity of 36–38%. It was supplied by Beijing Tong Guang Fine Chemicals Company. Sodium nitrite was of analytical reagent grade with a mass fraction purity of $\geq 99\%$. Sodium hydroxide was of analytical reagent grade with a mass fraction purity of $\geq 96\%$, and it was supplied by Shanghai Macklin Biochemical Co., Ltd.

2.2. Preparation of the reactant solution

Solution A: sodium nitrite (0.0494 mol) was dissolved in deionized water (400 mL) in a 1 L beaker.

Solution B: red base KD (0.0480 mol) was dissolved in deionized water (300 mL) in a 500 mL beaker, and concentrated hydrochloric acid (0.144 mol) was added into the beaker with stirring to form suspensions (as shown in Fig. 1). After that, the suspensions were replenished to a volume of 400 mL with deionized water.

Solution C: sodium 6-hydroxynaphthalene-2-sulfonate (0.0442 mol) and sodium hydroxide (0.217 mol) were dissolved in deionized water (400 mL) in a 1 L beaker.

Because the concentration of the reactants in the experiments was changed occasionally, the above was just one of the used ratios.

2.3. Experimental procedure of the continuous-flow process

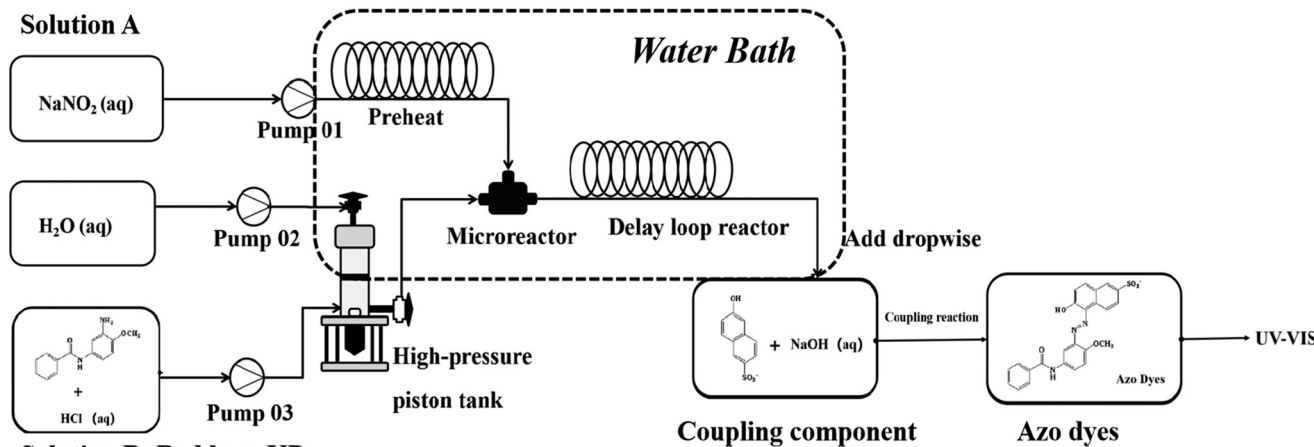
As shown in Fig. 2, solution A (NaNO_2) was conveyed into capillaries (PTFE, 2.0 mm inner diameter, 3.0 mm outer diameter) by constant-flow pumps (pump01, Beijing Satellite Manufacturing Co., Ltd.). Since solution B was a suspension, it was not suitable for the transportation by a constant-flow pump. In this system, solution B was firstly conveyed into a high-pressure piston kettle with stirring *via* a peristaltic pump (pump 03, Beijing Satellite Manufacturing Co., Ltd.). Then, the constant-flow pump (pump 02, Beijing Satellite Manufacturing Co., Ltd.) was used to convey water to the top of the high-pressure piston kettle. The water squeezed the piston and pressed out solution B into the microreaction system to react with solution A. A delay loop tube (PTFE, 2.0 mm inner diameter, 3.0 mm outer diameter) was connected to the outlet of the membrane dispersion microreactor. The diazotization reaction of red base KD occurred inside the microreactor and the delay loop tube. Both the microreactor and delay loop tube were submerged in a water bath to control the reaction temperature. The reaction time was controlled by changing the length of the delay loop tube.

The mixture solution from the outlet was directly added dropwise to the excess coupling component (solution C, 10 mL) that was stored in centrifuge tubes to quench the diazotization reaction. Then, as illustrated in Fig. 2, azo dyes were obtained through the diazo-coupling reaction.^{8,21} The concentration of the generated azo dye was quantified by UV-visible spectroscopy. Based on the quantitative relationship between the concentration of the diazonium salts and the azo dyes, the yield of the diazotization reaction could be obtained. In order to ensure the complete reaction between the diazonium salts and the coupling components to form azo dyes, the mixture solutions after the azo-coupling reaction were analyzed *via* the filter paper percolation ring test. This method was used for the rapid detection of diazonium salts, and their detection process was reported in the literature.²²

Fig. 3 shows the schematic diagram and photo of the high-pressure stainless-steel piston kettle. Water could be conveyed to the top of the high-pressure piston kettle using a constant-flow pump for the purpose of squeezing the piston and pressing out the suspensions. Simultaneously, a



Fig. 1 The preparation process of solution B.



Solution B: Red base KD hydrochloride suspensions

The diazotization and azo-coupling reaction

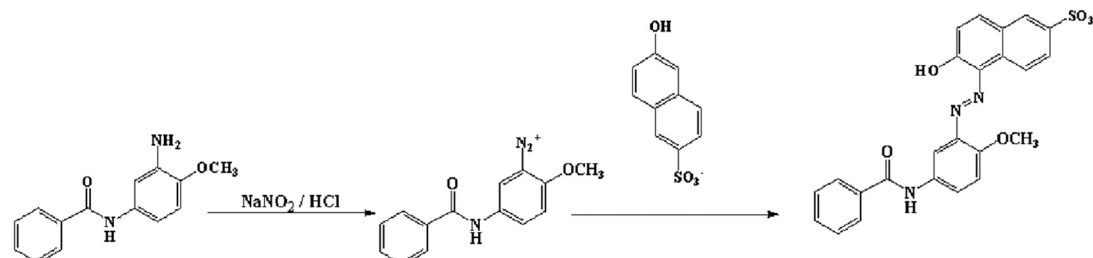


Fig. 2 Experimental setup for the continuous-flow diazotization reaction of red base KD.

magnetic stirring controller was used to control the speed of the magnetic stirrer in order to ensure the uniform distribution of the suspensions.

The schematic diagram and photo of the membrane dispersion microreactor are shown in Fig. 4, and it is also fabricated from stainless steel material. Solution A was dispersed by the membrane as a dispersed phase and solution B flowed continuously in the microchannel as a

continuous phase. The diameter of the membrane pore was 1 μm , and the dimension of the microchannel was 10 mm (length) \times 2 mm (wide) \times 0.33 mm (height).

2.4. Sample analysis

2.4.1 Standard working curve method for measuring the concentration of the azo dye. For the quantitative detection of the azo dyes synthesized by the azo-coupling reaction, the

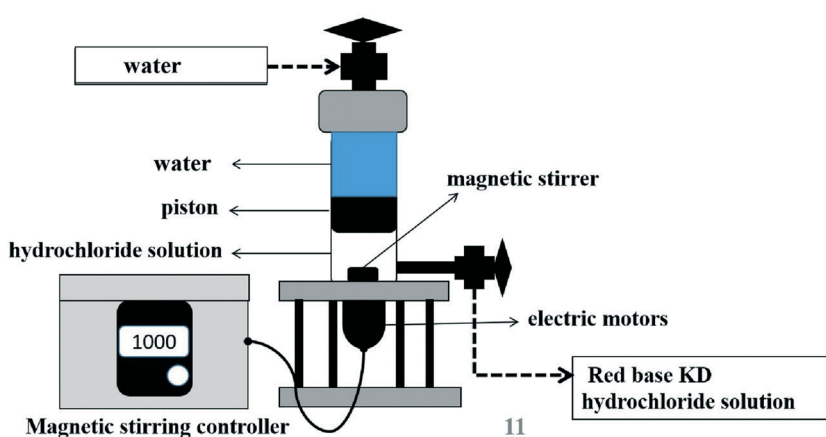


Fig. 3 Schematic diagram and photo of the high-pressure piston kettle.

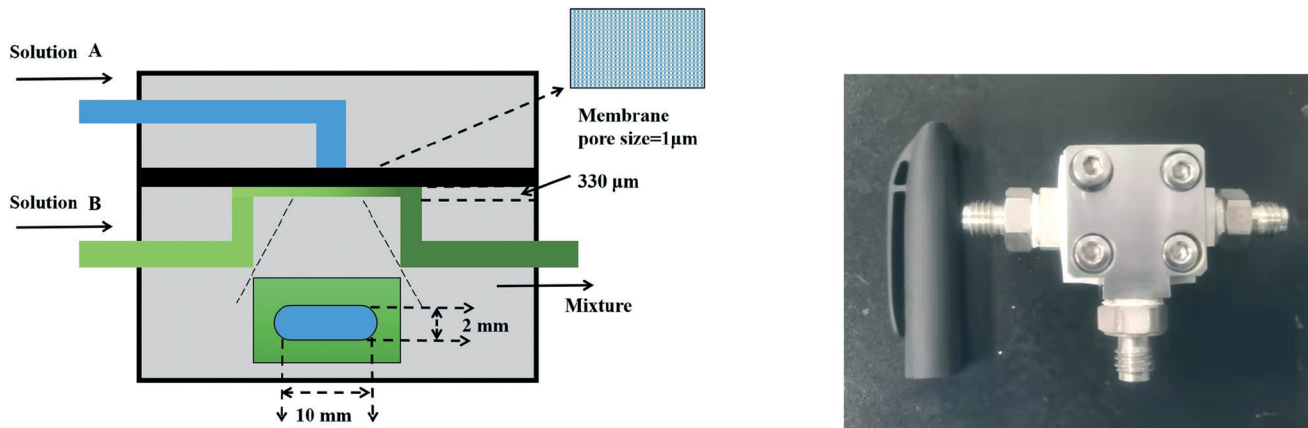


Fig. 4 Schematic diagram and photo of the membrane dispersion microreactor.

azo dyes were first synthesized by the batch process (as shown in 1 (1–3) in the ESI†), and the crude products were then purified to obtain the azo dye standards. The purity of the azo dye standard was about 98.5%, as measured by high performance liquid chromatography (as shown in Fig. S1 in the ESI†). The relative molecular mass of the product was measured to be 476.09 according to the results of mass spectrometry, which was similar to the value of 476.51 from theoretical calculation (as shown in Fig. S2 in the ESI†). Furthermore, the UV-visible spectroscopy results of the azo dyes were also detected. As shown in Fig. 5, the azo dye aqueous solution had a maximum absorption peak at a wavelength of 491 nm, and the coupling component had no absorbance at this wavelength.

Then, different concentrations of the azo dye standards were dissolved in deionized water, and the corresponding absorbance was measured by UV-visible spectroscopy at a wavelength of 491 nm. The standard working curve could be obtained from the standard products (as shown in Fig. S3 in the ESI†). The linear equation was described by eqn (1):

$$Y = 0.0296X + 0.01, \quad R^2 = 0.9996 \quad (1)$$

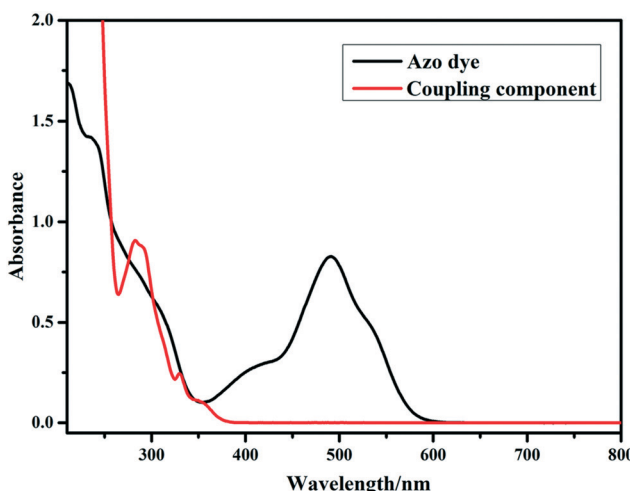


Fig. 5 UV-vis absorption curve of the azo dye standards.

where X is the concentration of the azo dye standards (mg L^{-1}) and Y is the absorbance.

In addition, both the precision experiments and reproducibility experiments were performed for the above mentioned measurement method (as shown in Table S1 and S2 in the ESI†). The results show that for the precision experiments, the relative standard deviation (RSD) of the azo dye concentration is 0.12%, and for the reproducibility experiments, the RSD of the azo dye concentration is 0.69%. Both values do not exceed 1%, proving that the precision and reproducibility of the method are satisfactory.

2.4.2 Calculation of the diazonium salt yield. As shown in Fig. 2, the chemical equation of diazotization and azo-coupling reaction showcases that the mole ratio of diazonium salt to azo dye should be 1:1. Therefore, the concentration of the diazonium salt can be calculated by the concentration of azo dye, which can be obtained from the standard working curve. Finally, the yield of the diazonium salt can be calculated according to eqn (2). In operation, the collected azo dye products should be diluted 100 times before analysis.

$$\text{yield} = \frac{c_D}{c_N} \times 100\% \quad (2)$$

where c_D (mg L^{-1}) is the actual concentration of the diazonium salt, c_N (mg L^{-1}) is the theoretical concentration of the diazonium salt, calculated by the concentration of red base KD.

3. Results and discussion

3.1. Optimization of experimental conditions in the microreaction system

3.1.1 Effects of the volume flow rate of the reactants on the yield of the diazotization reaction. In this section, the effects of different volume flow rates of the reactants on the yield of the diazotization reaction were studied in detail. The volume flow rates of solution A (NaNO_2) and solution B (red base KD + HCl) were varied from 15 to 25 mL min^{-1} . As demonstrated in Fig. 6, despite the yield of the diazotization

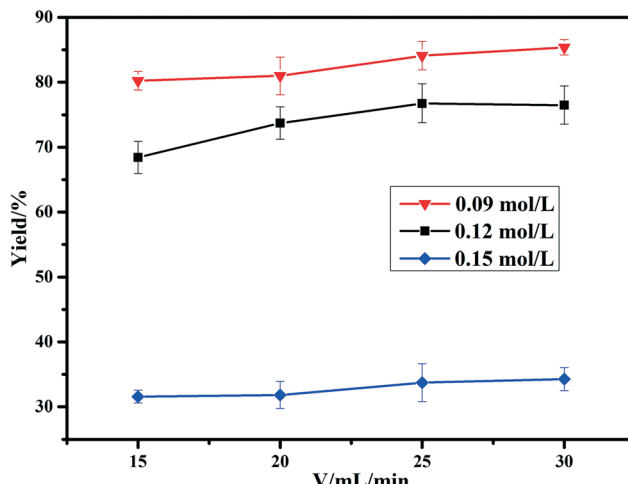


Fig. 6 Effects of the volume flow rates of the reactants on the yield of the diazotization reaction (reaction time (t) = 21.2 s; reaction temperature (T) = 25 °C).

reaction increasing along with the increase in the volume flow rates, the increase is found to be rather insignificant. When both the volume flow rates of solution A and solution B surpass 25 mL min^{-1} , the yield reaches its plateau. The mixing effects can be improved by increasing the volume flow rates, which in turn increases the rate of the diazotization reaction. Unfortunately, the results show that the mixing effect is not the main factor affecting the reaction process.

3.1.2 Effects of different reaction temperatures on the yield of the diazotization reaction. The reaction temperature was also considered, and it was varied from 15 to 35 °C to study the effects on the yield of diazotization reactions. Fig. 7 shows that the yield of the diazotization reaction is significantly affected by the reaction temperature. When the temperature is increased from 15 to 25 °C, the yield greatly

increases. When the reaction temperature is set at 25 °C, the yield reaches its peak. After the temperature is increased to 30 °C, the yield remains stable, or even slightly decreases. When the reaction temperature reaches 35 °C, the yield starts to showcase a downward trend. In fact, the increase in the reaction temperature promotes the dissolution of hydrochloride crystals^{23,24} and accelerates the rate of the diazotization reaction. However, when the reaction temperature exceeds 30 °C, the yield of the diazotization reaction decreases due to the thermal instability of diazonium salts. Therefore, for the continuous-flow diazotization synthesis process, the optimal reaction temperature is 25 °C.

3.1.3 Effects of different concentrations of red base KD and reaction time on the yield of the diazotization reaction.

Fig. 8 shows that the yield of the diazotization reaction increases with the reaction time increasing at different concentrations of red base KD (0.09–0.15 mol L⁻¹) and it also shows that at the same reaction time, the higher the concentration of red base KD, the lower the diazotization reaction yield. According to the kinetic equation of the diazotization reaction, the reaction rate should be proportional to the concentration of each reactant at the same temperature. The above results contradict with the theoretical model described by the kinetic equation. This means that the solid-liquid mass transfer process significantly affects the diazotization reaction.

3.2. Characterization of the agglomeration of the suspensions and optimization of the suspension preparation process

3.2.1 Microscopic state of the suspensions at different concentrations of red base KD. In order to verify the above theoretical calculations, the micrographs of the suspensions

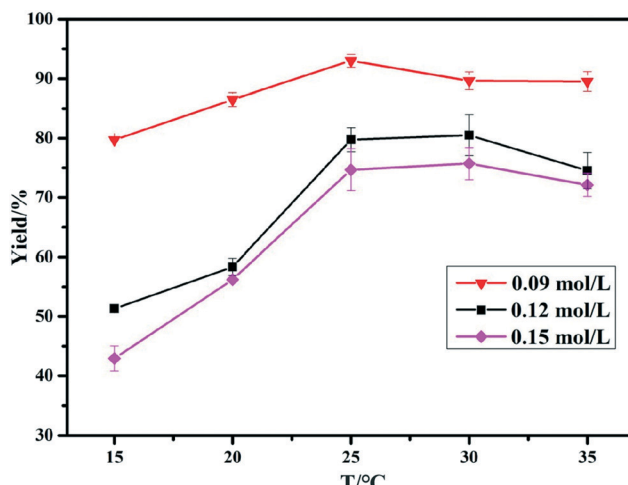


Fig. 7 Effects of the reaction temperature on the yield of the diazotization reaction ($V(\text{solution A}) = V(\text{solution B}) = 20 \text{ mL min}^{-1}$; reaction time (t) = 21.2 s).

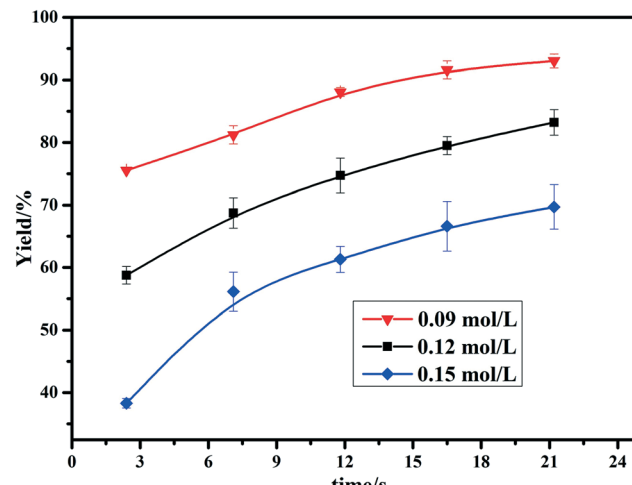


Fig. 8 The yield of the diazotization reaction at different reaction times and different concentrations of the suspensions ($V(\text{solution A}) = V(\text{solution B}) = 20 \text{ mL min}^{-1}$; reaction temperature (T) = 25 °C).

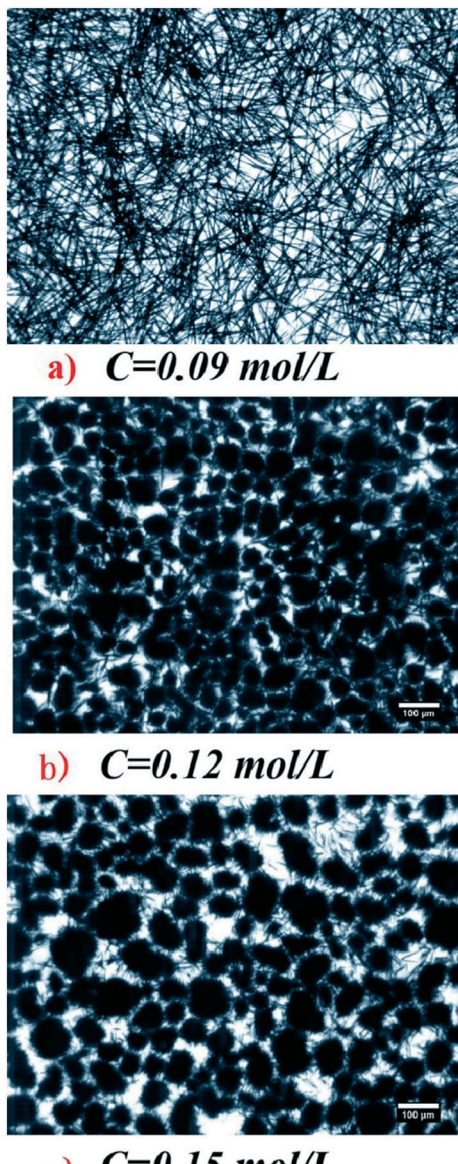


Fig. 9 The micrographs of red base KD hydrochloride and the particle size distribution and mean diameters at different concentrations: a) the micrographs of red base KD hydrochloride at 0.09 mol L^{-1} ; b) the micrographs of red base KD hydrochloride at 0.12 mol L^{-1} ; c) the micrographs of red base KD hydrochloride at 0.15 mol L^{-1} ; d) the particle size distribution at 0.12 mol L^{-1} ; e) the particle size distribution at 0.15 mol L^{-1} ($\text{C}(\text{HCl})/\text{C}(\text{red base KD}) = 3:1$).

were taken at different concentrations of red base KD. Fig. 9(a–c) show that crystals aggregate into particles when the concentration of red base KD increases from 0.09 mol L^{-1} to both 0.12 mol L^{-1} and 0.15 mol L^{-1} . Furthermore, the diameters of the particles in the micrographs were also measured using Nano Measurer 1.2. Here, the long diameter was taken as the statistics in the case of elliptical particles. According to the micrographs, the number of particles counted was more than 50. Both the particle size distribution and calculated mean diameters are shown in Fig. 9(d and e). In addition, the micrographs of the suspensions with concentrations of 0.105 mol L^{-1} and 0.18 mol L^{-1} were also obtained, and the mean diameters of particles were also calculated. The results in Fig. 10 show that when the

concentration exceeds 0.105 mol L^{-1} , the higher the concentration, the larger the mean diameters of the particles formed by agglomeration.

3.2.2 Effects of the concentrations of hydrochloric acid and red base KD on crystal agglomeration. In order to solve the problem of crystal agglomeration, we discuss two factors that may affect the crystal agglomeration in this section: 1) the concentration of hydrochloric acid; 2) the concentration of red base KD.

Fig. 11 shows that the concentration of hydrochloric acid has a great influence on the agglomeration process of the red base KD hydrochloride crystals. When the concentration of hydrochloric acid is less than 0.35 mol L^{-1} , red base KD hydrochloride crystals do not agglomerate and retain the

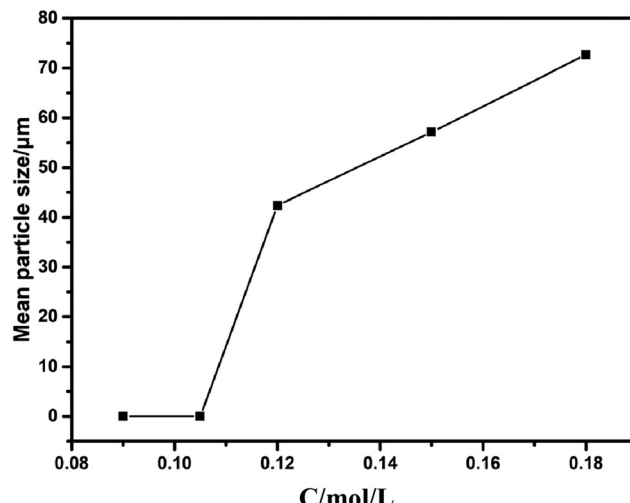


Fig. 10 Mean particle sizes (diameter) at different concentrations of red base KD.

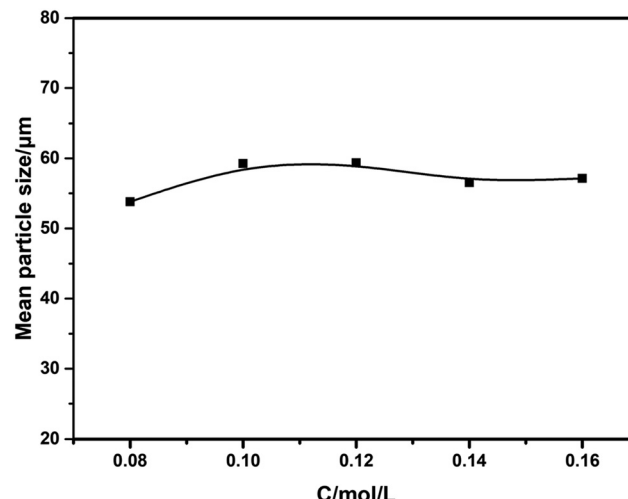


Fig. 12 Effects of different red base KD concentrations on the mean particle size of agglomerated particles ($C(\text{HCl}) = 0.45 \text{ mol L}^{-1}$).

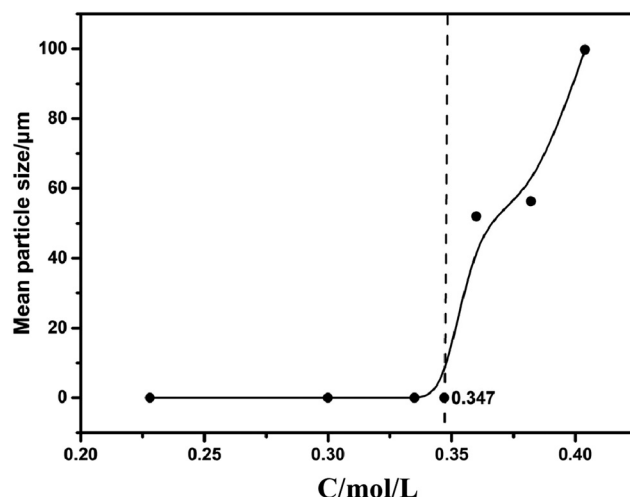


Fig. 11 Effects of different hydrochloric acid concentrations on the mean particle size of agglomerated particles ($C(\text{red base KD}) = 0.15 \text{ mol L}^{-1}$).

needle-like structure. When the concentration of hydrochloric acid is greater than 0.35 mol L^{-1} , agglomeration occurs in the suspensions. The agglomerated mean particle size increases as the concentration of hydrochloric acid increases. From the literature,²⁵ we know that higher supersaturation induces a higher crystal growth rate and the self-adhesion of suspended particles. Furthermore, Puela *et al.*²⁶ found that when the degree of supersaturation was relatively low, the growth rate of these organic crystals between the layers on the side was very slow. When the degree of supersaturation was high enough, the growth of the crystals competed with the secondary nucleation. The results of electron microscopy and atomic force microscopy in the literature showed that the agglomeration of needle-like crystals was due to the oriented crystallization of their respective components and the nucleation process was very rapid and random. In our

experiments, the increase in the concentration of hydrochloric acid improved the supersaturation of red base KD hydrochloride, which led to the occurrence of agglomeration.

Fig. 12 shows that when the concentration of hydrochloric acid is constant, the mean agglomerated particle sizes of the suspensions remain approximately the same at different concentrations of red base KD. The concentration of red base KD was varied from 0.08 mol L^{-1} to 0.16 mol L^{-1} while maintaining the concentration of hydrochloric acid at 0.45 mol L^{-1} . The concentration ratio of red base KD to hydrochloric acid was $1:(5.6\text{--}2.8)$, the concentration of hydrochloric acid had been kept in excess. Red base KD hydrochloride was always in a supersaturated state during the formation of hydrochloride crystals. Therefore, the concentration of hydrochloric acid is the most important factor affecting the agglomeration of red base KD hydrochloride crystals. Such an adverse phenomenon could prevent the agglomeration of red base KD hydrochloride crystals by reducing their supersaturation in the hydrochloric acid solution.

3.2.3 The different preparation processes of the red base KD hydrochloride suspensions. For solving the problem about the agglomeration of red base KD hydrochloride crystals, we added concentrated hydrochloric acid in several sequential additions to reduce the supersaturation of red base KD hydrochloride in the hydrochloric acid solution. Different preparation processes of the red base KD hydrochloride suspensions are shown in Fig. 13, and there were different dissolution phenomena for two processes: (1) sequentially adding an equal amount of acid three times; (2) adding all acid at once. The total mass of concentrated hydrochloric acid used in both processes was the same. When sequentially adding an equal amount of acid three times, the partial dissolution of red base KD occurred. After each addition of acid, the solution was in the state of suspension, and the micrograph showed that there was no

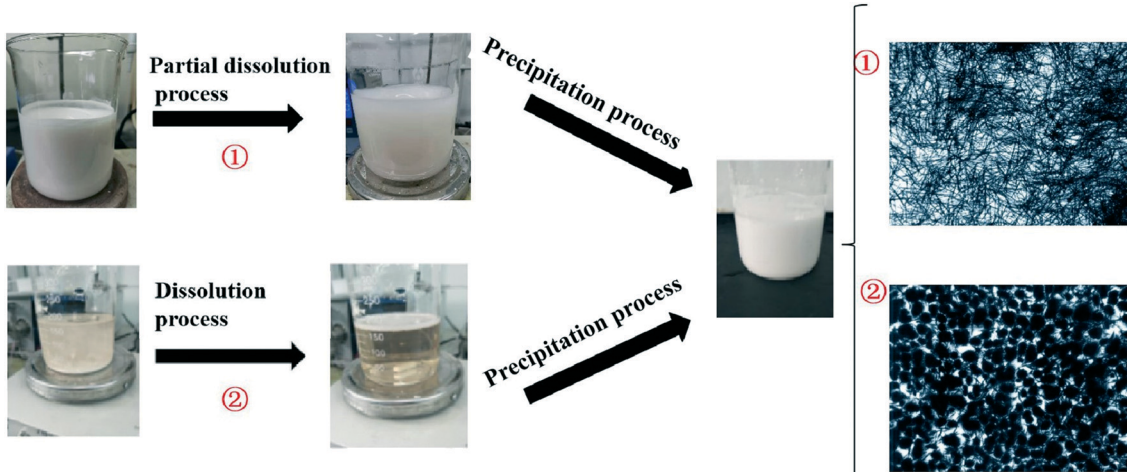


Fig. 13 Different preparation processes of the red base KD hydrochloride suspensions: (1) adding an equal amount of acid three times; (2) adding all acid at once.

agglomeration in the suspension. In contrast to the above phenomenon, there was complete dissolution when adding all acid at once. In this case, the solution was first clear, then quickly crystallized out. The micrograph of the suspension showed obvious agglomeration. Fig. 14 shows that the concentration of hydrogen ions varies with time for different acid addition processes.

3.3. Solid–liquid reaction model

In this part, a solid–liquid reaction model was used to describe the diazotization reaction between the red base KD hydrochloride crystal and sodium nitrite solution. According to the mechanism of the diazotization reaction,²⁷ we could know that the reactant that reacted with nitrous acid was mainly free aromatic amine, not the hydrochloride of aromatic amine. Therefore, the hydrochloride of aromatic amine needs to be dissolved to form free aromatic amine.

Then, the diazotization reaction was carried out between the free aromatic amine and nitrous acid. The reaction process was as follows:



According to the experimental results, the dissolution and diffusion process of the aromatic amines could be considered as a rate-limiting step, and its speed was much slower than the rate of the diazotization reaction. Therefore, for the spherical particles formed by agglomeration, the models in the literature²⁸ were used to describe the dissolution and diffusion reaction process.

As shown in Fig. 15(a), we assumed that solid A had certain solubility in the liquid reactant and the diazotization reaction occurred in very close vicinity of the solid surface but in the liquid phase. The choice of this reaction location could be derived from the reaction mechanism.²⁷ The solid–liquid reaction process included the following three steps.²⁹ First, the liquid phase reactant B (HNO_2) diffused to the vicinity of solid A (red base KD hydrochloride), which was a homogeneous diffusion process. Then, solid A dissolved and there was a free aromatic amine layer near the solid surface, which was a solid–liquid dissolution and diffusion process. Finally, reactant B reacted with the free amine produced by the dissolution of solid A to form the diazonium salt (AB).

Referring to Fig. 15(b), let the original radius be r_0 . At time t the interface had spread inwards a distance x , leaving a sphere of reactant A of radius r . According to the model in the literature,²⁸ it could be known that the expression of the spherical particle solid–liquid diffusion controlled equation was as follows:

$$\left(1 - (1 - \alpha)^{1/3}\right)^2 = \frac{k_1}{(r_0)^2} t = k't \quad (3)$$

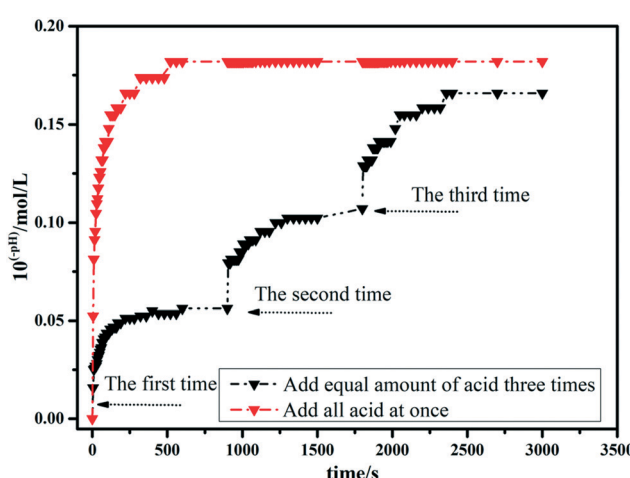


Fig. 14 Hydrogen ion concentration versus time curve for different acid addition processes.

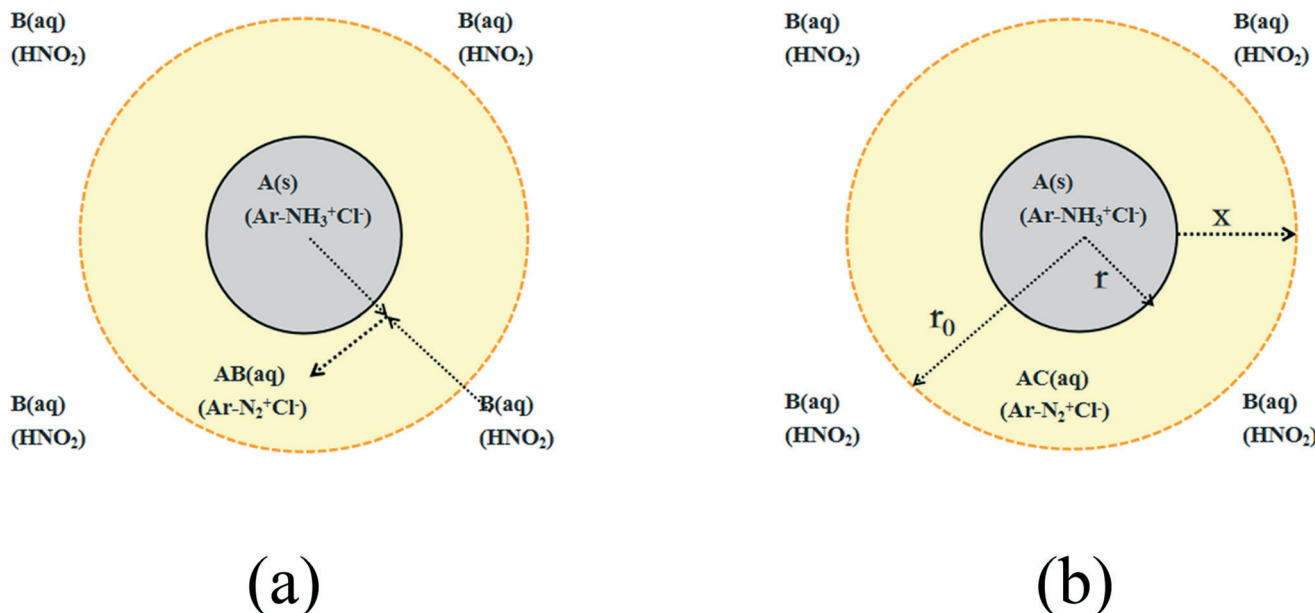


Fig. 15 Schematic representation of spherical granular solids in a sea of liquid: a) schematic diagram of solid–liquid reaction process; b) schematic diagram of model parameters.

k' : solid-liquid diffusion rate constant; α : the conversion of solid A; t : reaction time.

Furthermore, for the diazotization reaction process, we could obtain the chemical reaction rate equation from the literature:²⁷

$$-\frac{dC_B}{dt} = k_1 C_B C_A \quad (4)$$

k_1 : chemical reaction rate constant; C_A : the concentration of free aromatic amines; C_B : the concentration of the nitrous acid solution.

On the other hand, the consumption rate of B ($-dC_B/dt$) in the unit volume of solution B according to the diffusion of B to the interface in the liquid film near solid A could be written as:

$$-\frac{dC_B}{dt} = k_B(C_B - C_{BS}) \quad (5)$$

k_B : the mass transfer coefficients of B; C_{BS} : the concentration of B at the liquid film near solid A.

According to the above process, we can obtain that the reaction rate constant of the whole process consists of three parts:

$$\frac{1}{k} = \frac{1}{k'} + \frac{1}{k_p} + \frac{1}{k_s} \approx \frac{1}{k'} \quad (6)$$

For needle-shaped crystals, we assumed that it was a cylindrical solid (as shown in Fig. 16). According to the derivation in the literature,²⁸ the solid-liquid mass transfer controlled equation was as follows:

$$\left(1 - (1 - \alpha)^{1/2}\right)^2 = \frac{k_2}{r_{\alpha}^2} = k'_2 t \quad (7)$$

As shown in Fig. 17, the plots of $(1 - (1 - \alpha)^{(1/2)})^2$ (for spherical granular solids) and $(1 - (1 - \alpha)^{(1/3)})^2$ (for needle-like solids) versus t are straight lines. The values of k are the slopes of these linear equations. Table 1 shows fitting linear equations and slopes at different red base KD concentrations obtained from Fig. 17. It demonstrates that the value of k decreases with the increase of the concentrations of red base KD in Fig. 18. When the concentration of red base KD is increased from 0.09 mol L^{-1} to 0.12 mol L^{-1} , the value of k decreases from 0.0117 to 0.0072 , approximately reduced by 38% . When the concentration is increased from 0.12 mol L^{-1}

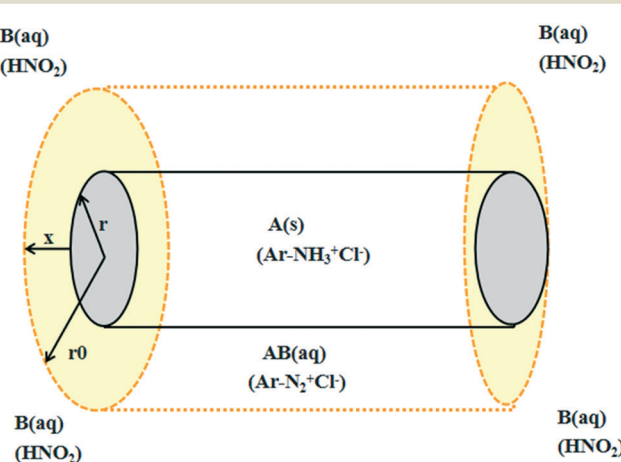
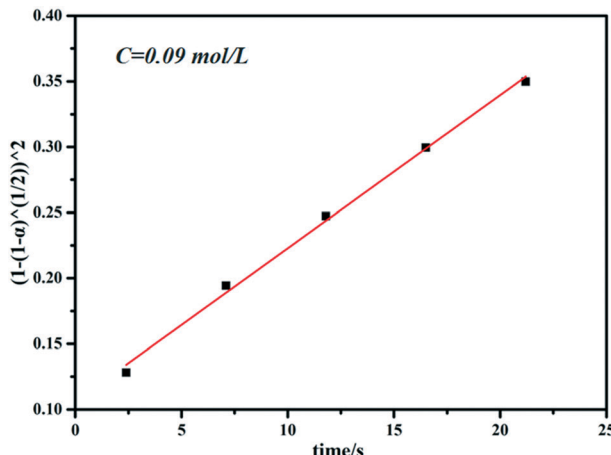
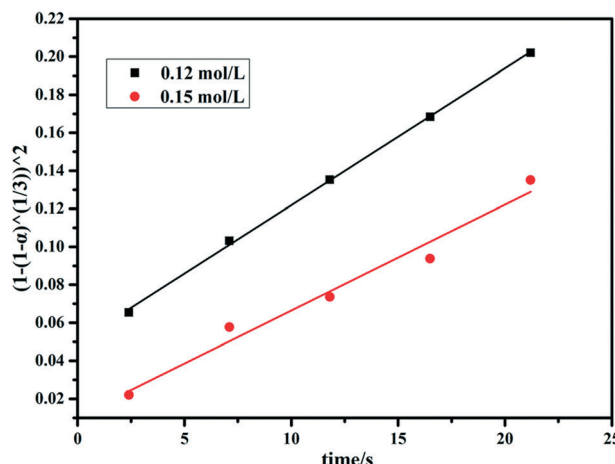


Fig. 16 Schematic representation of needle-like solids in a sea of liquid.



(a)



(b)

Fig. 17 The linear fitting equations: a) the plot of $(1 - (1 - \alpha)^{1/2})^2$ (for spherical granular solids) versus t at different concentrations of red base KD; b) the plot of $(1 - (1 - \alpha)^{1/3})^2$ (for needle-like solids) versus t at different concentrations of red base KD ($V(\text{solution A}) = V(\text{solution B}) = 20 \text{ mL min}^{-1}$; reaction temperature (T) = 25 °C).

to 0.15 mol L⁻¹, the value of k decreases from 0.0072 to 0.0056, approximately reduced by 22%.

The above results show that with the concentration of red base KD increasing, k significantly decreases, which leads to the decrease of the mass transfer rate between the solid and liquid. According to the above theoretical calculations, it can be considered that the red base KD hydrochloride crystals have agglomerated, which leads to the decrease of k .

3.4. Effects of different suspensions on the yield of the diazotization reaction

The above results showed that crystal agglomeration could be prevented by altering the suspension preparation process. Therefore, the sequential addition of hydrochloric acid was used to replace the original method of adding all the acids at once. For comparison, both methods were used to prepare the suspensions, which were used as reactants in the process of the diazotization reaction. Two different suspensions were obtained as follows:

Suspension (1): red base KD (0.048 mol/0.06 mol) was dissolved in deionized water (300 mL) in a 500 mL beaker, and concentrated hydrochloric acid (0.144 mol/0.18 mol) was added into the beaker while stirring to form a suspension. Afterwards, the suspension was replenished to a volume of 400 mL with deionized water.

Table 1 Fitting linear equations and slopes at different red base KD concentrations

Concentration(mol L ⁻¹)	Fitting equation	R ²
0.09	$Y = 0.0117X + 0.1066$	0.9970
0.12	$Y = 0.0072X + 0.0502$	0.9992
0.15	$Y = 0.0056X + 0.0011$	0.9740

Suspension (2): red base KD (0.048 mol/0.06 mol) was dissolved in deionized water (300 mL) in a 500 mL beaker, and the concentrated hydrochloric acid was divided into three equal portions. The first portion of hydrochloric acid (0.048 mol/0.06 mol) was added into the beaker while stirring to form a suspension. After stirring for 30 min, the second portion of concentrated hydrochloric acid (0.048 mol/0.06 mol) was added into the suspension and stirred for another 30 min. Lastly, the third portion of concentrated hydrochloric acid was added and stirred for 60 min. After stirring, the suspension was replenished to a volume of 400 mL with deionized water.

Fig. 19(a and b) shows that the yield of the diazotization reaction is increased when increasing the reaction time from 2.4 s to 21.2 s. Fig. 19(a) shows that the yield of the diazotization reaction using suspension (2) is 99.91% at a

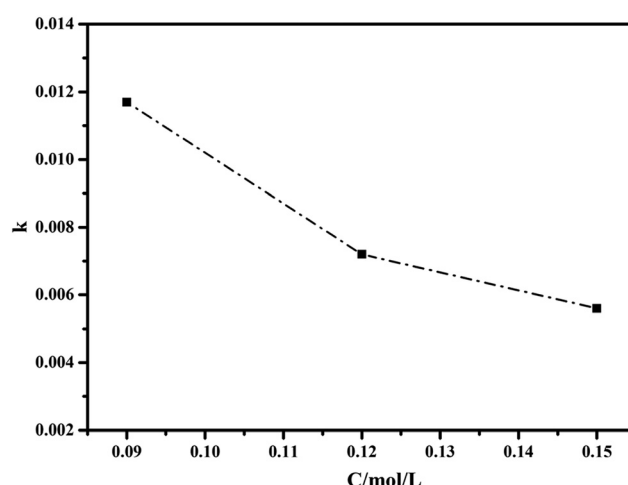
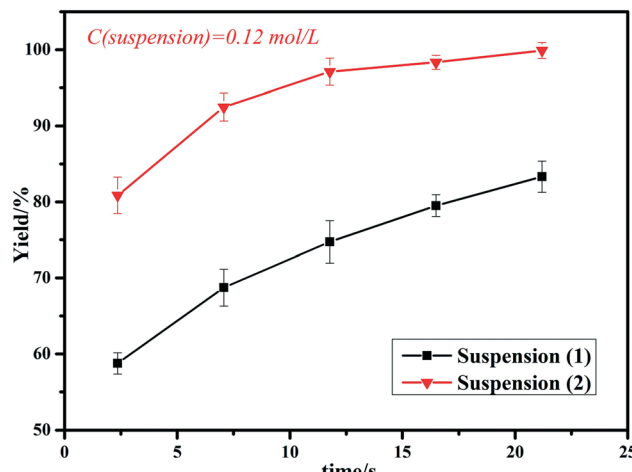
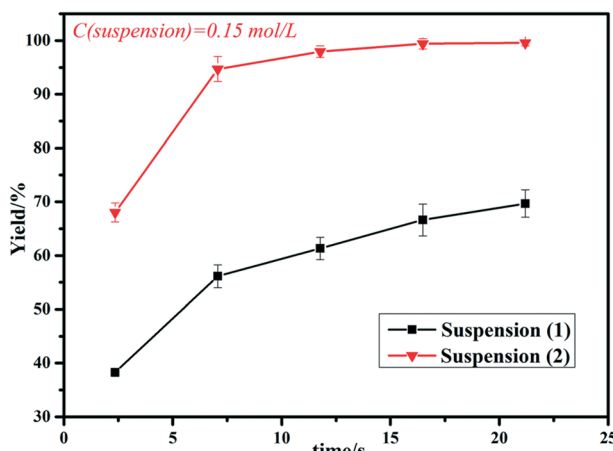


Fig. 18 The values of k at different red base KD concentrations.



(a)



(b)

Fig. 19 The yields of the diazotization reaction using different suspensions: (a) $C(\text{suspension}) = 0.12 \text{ mol L}^{-1}$; (b) $C(\text{suspension}) = 0.15 \text{ mol L}^{-1}$ ($V(\text{solution A}) = V(\text{solution B}) = 20 \text{ mL min}^{-1}$; reaction temperature (T) = 25 °C).

reaction time of 21.2 s and the concentration of red base KD of 0.12 mol L⁻¹, which was increased by 19.93% compared to the scenario using suspension (1) (83.31%). Fig. 19(b) shows that the yield of the diazotization reaction using suspension (2) is 99.58% at a reaction time of 21.2 s and the concentration of red base KD is 0.15 mol L⁻¹, which was increased by 42.89% compared to the scenario using suspension (1) (69.69%).

Fig. 20 shows the photos of diazonium salt solutions produced using two different suspensions, and the diazonium salts synthesized using suspension (2) are clearer than those using suspension (1). Furthermore, the scalability of the preparation method of the red base KD hydrochloride suspension was also studied (as shown in 3 in the ESI†) and the results demonstrated that the method of preparing the



(a)



(b)

Fig. 20 The photos of the diazonium salt produced using different suspensions: (a) using suspension (2); (b) using suspension (1) (reaction temperature (T) = 25 °C; $V(\text{solution A}) = V(\text{solution B}) = 20 \text{ mL min}^{-1}$; residence time (t) = 21.2 s).

Table 2 The comparison of the continuous-flow process and batch process

Operation process	Continuous-flow	Batch ³⁰
Reaction time	21.2 s	Hours
Reaction temperature	20–25 °C	0–5 °C
Yield	≥99%	Not provided

suspensions mentioned above had a certain degree of scalability.

3.5. The comparison of the continuous-flow process and batch process

In order to emphasize the advantages of the continuous-flow process, the comparison of two different operation processes was summarized. As shown in Table 2, the reaction time was greatly shortened by increasing the reaction temperature and using the superior mass and heat transfer characteristics of the continuous-flow system. The continuous-flow system could significantly reduce the energy consumption while enhancing the efficiency of production of the diazotization process. In addition, the realization of the diazotization reaction in the continuous-flow system as described in this work is readily adapted for other analogous reactions.

4. Conclusion

In summary, a microreaction system for the continuous-flow diazotization reaction of red base KD was developed in this work. After investigating the effect of reaction temperature, reactant volume flow, red base KD concentration and reaction time on the yield of the diazotization reaction, the optimal reaction conditions were obtained: reaction temperature (T) =

25 °C and reactant volume flow = 20 mL min⁻¹. According to the solid–liquid reaction model, we found that agglomeration of the hydrochloride crystals significantly affected the diazotization reaction in an adverse manner due to the solid–liquid mass transfer process. Then we explored the agglomeration phenomenon of the red base KD hydrochloride suspensions under different conditions and found that the agglomeration of suspensions could be prevented by reducing the supersaturation of red base KD hydrochloride in the hydrochloric acid solution. Finally, the yield of the diazotization reaction using the suspensions prepared by the new method was increased compared to the scenario using the original suspensions. A good yield of diazonium salt (99.91% and 99.58%) was achieved rapidly in only 21.2 s when the concentrations of red base KD were 0.12 mol L⁻¹ and 0.15 mol L⁻¹, respectively. Importantly, the diazotization reaction of the suspensions in the microreaction system was deeply studied. Compared to the conventional batch reactors, the continuous-flow microreaction system possesses numerous advantages including continuous operation, enhanced mixing, high safety performance and easy scale up. Consequently, the microreaction system developed in this work will be significant for the industrial production of diazonium salt intermediates as well as downstream fine chemical products.

Author contributions

F. J. Wang performed the experiments and wrote the draft of the manuscript, and all authors participated in revising the manuscript. J. H. Xu provided oversight to the project and secured funding.

Conflicts of interest

There are no conflicts to declare.

Acknowledgements

The authors gratefully acknowledge the support of the National Natural Science Foundation of China (21991100) for this work.

References

- N. Oger, E. Le Grogne and F. X. Felpin, Handling diazonium salts in flow for organic and material chemistry, *Org. Chem. Front.*, 2015, **2**, 590–614.
- F. Mo, G. Dong, Y. Zhang and J. Wang, Recent applications of arene diazonium salts in organic synthesis, *Org. Biomol. Chem.*, 2013, **11**, 1582–1593.
- L. He, G. Qiu, Y. Gao and J. Wu, Removal of amino groups from anilines through diazonium salt-based reactions, *Org. Biomol. Chem.*, 2014, **12**, 6965–6971.
- E. Merino, Synthesis of azobenzenes: the coloured pieces of molecular materials, *Chem. Soc. Rev.*, 2011, **40**, 3835–3853.
- F. J. Wang, J. P. Huang and J. H. Xu, Continuous-Flow Synthesis of the Azo Pigment Yellow 14 Using a Three-Stream Micromixing Process, *Org. Process Res. Dev.*, 2019, **23**, 2637–2646.
- F. M. Akwi, C. Bosma and P. Watts, A Facile Optimization of Diazotization and Phase Transfer Catalyzed Azo-Coupling Reactions in Microreactors, *J. Flow Chem.*, 2016, **6**, 73–79.
- R. C. R. Wootton, R. Fortt and A. J. De Mello, On-chip generation and reaction of unstable intermediates Monolithic nanoreactors for diazonium chemistry: Azo dyes, *Lab Chip*, 2002, **2**, 5–7.
- H. Pennemann, S. Forster, J. Kinkel, V. Hessel, H. Löwe and L. Wu, Improvement of Dye Properties of the Azo Pigment Yellow 12 Using a Micromixer-Based Process, *Org. Process Res. Dev.*, 2005, **9**, 188–192.
- Z. Q. Yu, Y. W. Lv, C. M. Yu and W. K. Su, Continuous flow reactor for Balz-Schiemann reaction: a new procedure for the preparation of aromatic fluorides, *Tetrahedron Lett.*, 2013, **54**, 1261–1263.
- Z. Q. Yu, X. Ye, Q. L. Xu, X. X. Xie, H. Dong and W. K. Su, A Fully Continuous-Flow Process for the Synthesis of p-Cresol: Impurity Analysis and Process Optimization, *Org. Process Res. Dev.*, 2017, **21**, 1644–1652.
- C. A. Shukla, A. A. Kulkarni and V. V. Ranade, Selectivity engineering of the diazotization reaction in a continuous flow reactor, *React. Chem. Eng.*, 2016, **1**, 387–396.
- S. Partington and S. P. Waldrum, Runaway reaction during production of an azo dye intermediate, *Process Saf. Environ. Prot.*, 2002, **80**, 33–39.
- J. P. Huang, F. N. Sang, G. S. Luo and J. H. Xu, Continuous synthesis of Gabapentin with a microreaction system, *Chem. Eng. Sci.*, 2017, **173**, 507–513.
- W. Q. Yuan, S. Q. Zhou, Y. Y. Jiang, H. H. Li and H. D. Zheng, Organocatalyzed styrene epoxidation accelerated by continuous-flow reactor, *J. Flow Chem.*, 2020, **10**, 227–234.
- A. A. Kulkarni, Continuous flow nitration in miniaturized devices, *Beilstein J. Org. Chem.*, 2014, **10**, 405–424.
- U. Hirotsugu, T. Yutaka, N. Aiichiro, O. Hideho, N. Toshiki and J. I. Yoshida, Generation and Reactions of o-Bromophenyllithium without Benzyne Formation Using a Microreactor, *J. Am. Chem. Soc.*, 2007, **129**, 3046–3047.
- M. Movsisyan, E. I. P. Delbeke, J. K. E. T. Berton, C. Battilocchio, S. V. Leyb and C. V. Stevens, Taming hazardous chemistry by continuous flow technology, *Chem. Soc. Rev.*, 2016, **45**, 4892–4928.
- R. A. Maurya, P. H. Hoang and D. Kim, Efficient and continuous monoacetylation with superior selectivity of symmetrical diamines in microreactors, *Lab Chip*, 2012, **12**, 65–68.
- J. D'Attoma, T. Camara, P. L. Brun, Y. Robin, S. Bostyn, F. Buron and S. Routier, Efficient Transposition of the Sandmeyer Reaction from Batch to Continuous Process, *Org. Process Res. Dev.*, 2017, **21**, 44–51.
- A. Pawlowska-Zygarowicz, R. Kukawka, H. Maciejewski and M. Smiglak, Optimization and intensification of hydrosilylation reactions using a microreactor system, *New J. Chem.*, 2018, **42**, 15332–15339.
- F. J. Wang, J. P. Huang and J. H. Xu, Continuous-flow synthesis of azo dyes in a microreactor system, *Chem. Eng. Prog.*, 2018, **127**, 43–49.

- 22 F. J. Wang, Y. C. Ding and J. H. Xu, Continuous-flow synthesis of pigment red 146 in a microreactor system, *Ind. Eng. Chem. Res.*, 2019, **58**, 16338–16347.
- 23 D. D. Han, X. N. Li, H. S. Wang, Y. Wang, S. C. Du, B. Yu, Y. M. Liu, S. J. Xu and J. B. Gong, Determination and correlation of pyridoxine hydrochloride solubility in different binary mixtures at temperatures from (278.15 to 313.15) K, *J. Chem. Thermodyn.*, 2016, **94**, 138–151.
- 24 P. S. Zhang, Y. M. Wan, C. Zhang, R. Zhao, J. Sha, Y. Li, T. Li and B. Z. Ren, Solubility and mixing thermodynamic properties of levamisole hydrochloride in twelve pure solvents at various temperatures, *J. Chem. Thermodyn.*, 2019, **139**, 105882.
- 25 I. Seysseicq, S. Veesler, R. Boistelle and J. M. Lamérant, Agglomeration of gibbsite Al(OH)₃ crystals in Bayer liquors. Influence of the process parameters, *Chem. Eng. Sci.*, 1998, **53**, 2177–2185.
- 26 F. Puela, E. Verduranda, P. Taulelleb, C. Bebona, D. Colsona, J.-P. Kleina and S. Veeslerb, Crystallization mechanisms of acicular crystals, *J. Cryst. Growth*, 2008, **310**, 110–115.
- 27 O. Masaya and O. Yoshiro, Kinetics of the Diazotization of Anilines, *J. Am. Chem. Soc.*, 1953, **75**, 5175–5177.
- 28 C. F. Dickinsona and G. R. Healb, Solid-liquid diffusion controlled rate equations, *Thermochim. Acta*, 1999, **340**, 89–103.
- 29 H. Grénman, T. Salmi and D. Y. Murzin, Solid-liquid reaction kinetics-experimental aspects and model development, *Rev. Chem. Eng.*, 2011, **27**, 53–77.
- 30 D. J. Lu and J. C. Zhang, Synthesis and Modification of C. I. Pigment Red 146, *Ranliao Yu Ranse*, 2007, **44**, 6–8.